32ND INTERNATIONAL COSMIC RAY CONFERENCE, BEIJING 2011

High-energy electron observations from 30 GeV to 3 TeV with emulsion chambers

TADASHI KOBAYASHI[1], YOSHIKO KOMORI[2], KENJI YOSHIDA[3], JUN NISHIMURA[4]
[1]*Department of Physics, Aoyama Gakuin University, Sagamihara 229-8558, Japan*
[2]*Kanagawa University of Human Services, Yokosuka 238-0013, Japan*
[3]*College of Systems Engineering and Science, Shibaura Institute of Technology, Saitama 337-8570, Japan*
[4]*Institute of Space and Astronautical Science, JAXA, Sagamihara 229-8510, Japan*
komori-y@kuhs.ac.jp

Abstract: We have observed high-energy cosmic-ray electrons from 30 GeV to 3 TeV with emulsion chambers at balloon altitudes, accumulating the total exposure of 8.19 m^2.sr.day. In the observations, we have carried out particle identification event by event with a proton rejection power of 1×10^5 in TeV region, which is one of the outstanding capabilities of the emulsion chambers. The performance of the emulsion chambers was examined by accelerator beam tests at CERN-SPS and Monte-Carlo simulations. We also estimated the atmospheric electron spectra in a reliable way, and carried out on-board calibrations by using flight data. In the study of cosmic-ray electrons, it is indicated that high-energy electrons above a few 100 GeV are a powerful probe to identify nearby cosmic-ray sources and search for dark matter. In this paper, we present the final result of energy spectrum of high-energy cosmic-ray electrons observed with emulsion chambers in the energy range from 30 GeV to 3 TeV.

Keywords: Cosmic-ray electrons, Supernova remnants, Balloon

1 Introduction

High-energy cosmic-ray electrons cannot propagate far from the sources, because the electrons lose rapidly energy with an energy loss rate of the square of energy through the synchrotron radiation in the Galactic magnetic field and inverse Compton scattering with the interstellar photons in the Galaxy. Kobayashi *et al.* (2004) suggests that the energy spectrum of cosmic-ray electrons might have unique spectral structures in the TeV region due to the discrete effect of local sources [1]. This means that we can identify cosmic-ray electron sources from the electron spectrum in the TeV region. In addition, it is discussed that some dark matters may produce electron and positrons in the energy region of $\sim100 - 10$ TeV via dark matter annihilations or decaying dark matter (e.g. [2]). In particular, in the case of mono-energetic electrons and positrons from dark matter, although the propagation through the Galaxy would broaden the line, the observed electron and positron spectrum could still have a distinctive feature. Thus, the observations of high-energy electrons bring us unique information about sources and propagation of cosmic rays, and enable us to search for dark matter.

The difficulty of the electron observations originates from that the electron flux itself is very small and decreases with energy much more rapidly than that of protons because of the electro-magnetic energy loss by radiation. The electron flux is estimated to be ~1 % of protons at 10 GeV and ~0.1 % of protons at 1 TeV. Therefore, there are few observations of the electrons in the TeV region, since we need a long duration exposure with the detector that has a large geometrical factor, enough thickness, and powerful background rejections. Although ATIC-2 team reported the cosmic-ray electron spectrum up to a few TeV [3], the independent data analysis of ATIC-2 + ATIC-4 indicates large systematic errors on their electron spectra [4]. In spite of the large exposures of Fermi-LAT observations, the detector thickness of Fermi-LAT is insufficient to observe electrons in the TeV region [5]. While H.E.S.S. team reported the electron spectrum up to several TeV, which is provided by the indirect observations with ground-based imaging atmospheric Cherenkov telescopes [6], H.E.S.S. intrinsically has systematic errors on the reconstructed electron spectra arising from uncertainties in the simulation of hadronic interactions, the atmospheric model, and the absolute energy scale.

2 Observations

2.1 Detector

Emulsion chambers (ECC) consists of nuclear emulsion plates, X-ray films and lead plates. A nuclear emulsion plate is a methacrylate substrate $500-800$ μm thick, double coating of nuclear emulsion with $50 - 100$ μm thickness.

Nuclear emulsion plates are placed under lead plates. One or two X-ray films are inserted between a lead plate and a nuclear emulsion plate to allow rapid, naked-eye scanning for high-energy cascade showers, which produce dark spots in the films. Figure 1 shows a typical emulsion chamber configuration. The typical size and thickness of the detector are 40 cm $\times$ 50 cm, and 8 cm ($\sim$ 9 r.l.), respectively.

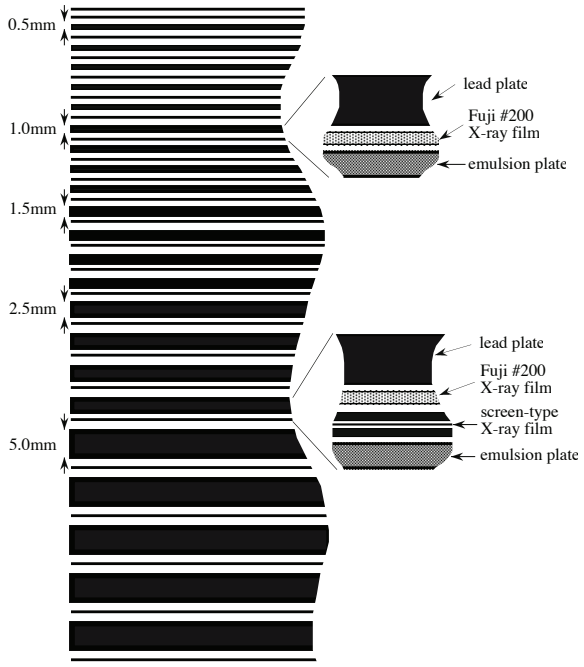

Figure 1: Typical configuration of the emulsion chamber in cross-sectional drawing from side view.

We measure the shower particles within a circle of 100 μm radius from shower axis. This means that we select the shower particles with higher energies, which suffered less multiple scattering in the chamber. Hence, the number of the shower particles drops off faster than for all shower particles. The shower maximum appears in $\sim$ 6 r.l. for 1 TeV electrons, while the maximum of the total number of shower particles appears in $\sim$ 12 r.l. for 1 TeV electrons. As a result, the energy of higher energy incident electrons can be determined with a thinner detector. Thus the emulsion chamber has the advantages of a wide field of view and thin thickness, compared with other detectors.

2.2 Balloon observations

We have observed cosmic-ray electrons with balloon-borne emulsion chambers in 14 flights between 1968 and 2001. The pressure altitude records for each flight correspond to residual atmospheric overburdens in the range from 4.0 g cm^{-2} to 9.4 g cm^{-2}. Figure 2 shows the total cumulative effective exposure $S\Omega_e T$ for primary electrons, which is 8.19 m-sr-day in the TeV region. In table 1, we summarize the series of experiments since 1968.

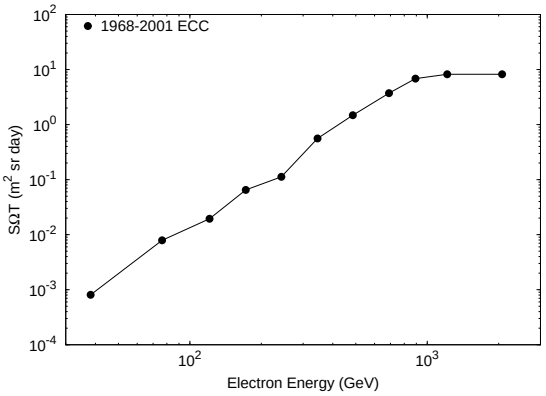

Figure 2: Total exposure $S\Omega_e T$ with electron energy.

Table 1: List of balloon flights

Flight	Area (m^2)	Time (min)	Altitude* (g cm^{-2})	$S\Omega_e T$ (m^2 sr s)
1968	0.05	380	6.1	1.826×10^3
1969	0.05	267	7.1	1.283×10^3
1970	0.05	1136	6.1	5.460×10^3
1973	0.20	833	8.2	1.934×10^4
1976	0.40	1526	4.0	7.084×10^4
1977	0.78	1760	4.5	1.2772×10^5
1979	0.80	1680	4.9	1.5389×10^5
1980	0.80	2029	7.8	1.8838×10^5
1984	0.20	576	9.2	5.330×10^3
1985	0.40	940	9.4	9.930×10^3
1988	0.20	647	7.1	2.948×10^3
1996	0.20	2092	4.6	4.874×10^4
1998	0.20	1178	5.6	2.729×10^4
1999	0.20	891	5.6	2.005×10^4
2001	0.20	1108	5.5	2.494×10^4

* Average altitude

3 Data analysis

3.1 Event identification

In emulsion chambers, it is possible to measure the location of shower tracks in each emulsion plate with a precision of $\sim$ 1 μm. In the balloon observations, we identify electron events among incoming cosmic-ray events, determine energy, and measure the depth of the first electron-positron pair of the electron-induced showers, so called the shower starting point. The incoming particles such as electrons, gamma-rays, protons, and heavier nuclei are identified by inspecting the shower starting points in detail.

The identification of electrons is carried out by the existence of a single track at the top of the emulsion chamber and a pair track with the opening angle less than 4 degree at the interaction point. Electron events also give the electro-magnetic shower without core structures. Gamma-ray events, which are also a pure electro-magnetic shower, start from a pair without a visible single track above the

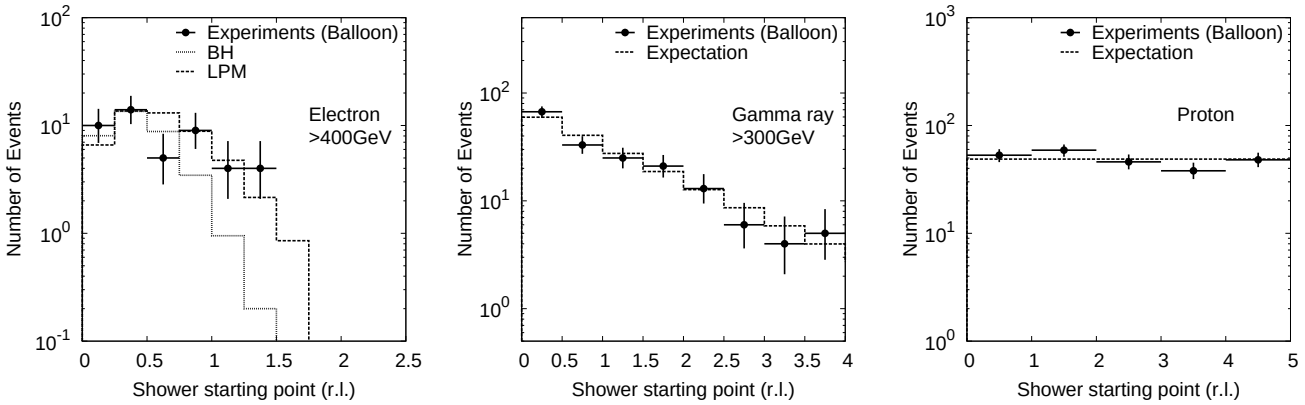

Figure 3: Shower starting point distributions for the observed electrons, gamma rays, and protons, compared to the expectations.

shower starting point. Although the incident track of a proton shower shows a single charged track like an electron, proton showers also have many secondaries at the shower starting point and often have multi core structures in the deep layers. Hadron showers of heavier nuclei such as helium are easily distinguished because the grain density of the incident track is larger than 4 times of a single charged track. As described in Nishimura *et al.* (1980) [7], the proton rejection power is estimated as high as 1×10^5, including the effect of the difference of the interaction m.f.p. between electron and proton, and the energy shift of protons.

The validity of event identification is checked by comparison with the expected shower starting points. We picked up the events that have the zenith angle below 60° and penetrate both the top and bottom side of the chamber. Figure 3 presents the shower starting point distributions of the balloon observations for electrons, gamma rays, and protons, compared to the expectations. As shown in Fig. 3, the shower starting point distributions show agreement with the expectations, providing a check on the reliability of the particle identification.

3.2 Energy determination

Electron energies were determined by counting the number of shower tracks in each emulsion plate within a circle of radius 100 μm centered on the shower axis. We derived the integrated track length from these counted tracks in each layer. The integrated track length is expected to be directly proportional to the shower energy. Our chamber structure is slightly different at each flight because of fluctuations of lead thicknesses and insertion of different types of X-ray films and screens. We calculated the shower development for each chamber using a Mote-Carlo simulation code called EPICS [8]. The incident electron energy is determined by these track lengths compared with the value estimated from the M.C. simulation for each chamber.

Results calculated using the EPICS code were confirmed by the emulsion chambers exposed to electron beams of 50 GeV and 200 GeV at CERN-SPS. Figure 4 shows longitudinal developments of the averaged number of shower tracks from the M.C. simulations, compared to the experimental data. As shown in Fig. 4, the determined energies with the simulations are consistent with the experiments for 50 GeV and 200 GeV electrons. Figure 5 shows the energy dependence of energy resolution from the simulations, compared to the experimental data for electrons of 50 GeV and 200 GeV. The energy resolution for the emulsion chamber is well represented by the form of

$$\frac{\sigma}{E} = [8.6\%^2(\frac{E}{100\mathrm{GeV}}) + 6.9\%^2 + 2.4\%^2(\frac{E}{100\mathrm{GeV}})]^{1/2}, \quad (1)$$

where E is the electron energy and σ is the standard deviation of energy determination.

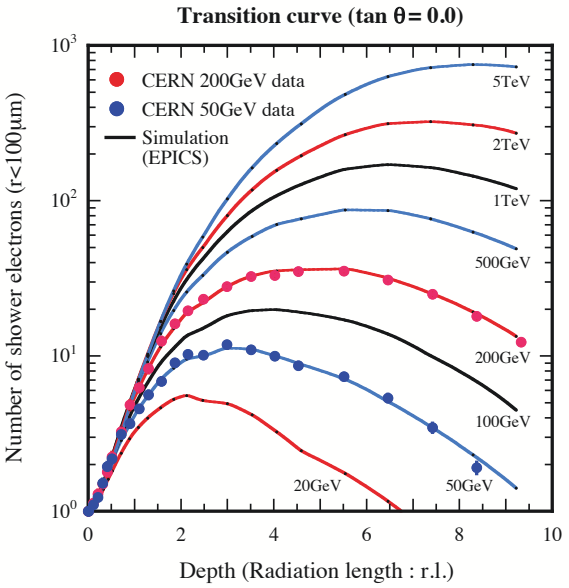

Figure 4: Longitudinal development of the averaged number of shower tracks within a radius of 100 μm from the simulations, compared to the experimental data.

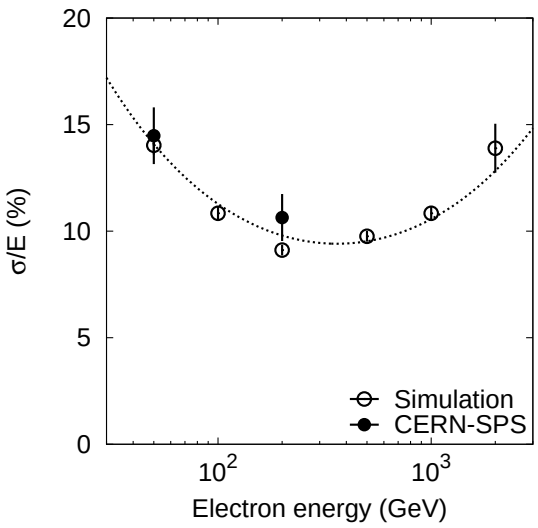

Figure 5: Energy dependence of energy resolutions with the emulsion chambers from the simulations, compared to the experimental data for electrons of 50 GeV and 200 GeV.

3.3 Electron energy spectrum

In balloon flight experiments, corrections to the observed cosmic-ray electron spectrum are necessary because of the residual overlying atmosphere. We corrected energy loss of primary electrons due to bremsstrahlung radiation in the overlying atmosphere, considering that the energy losses of electrons have broad distributions and the input electron spectrum is steeply sloped. We also estimated the atmospheric electron spectra in the reliable way without uncertainties from hadronic interaction models and primary cosmic-ray spectra. Since atmospheric electrons are produced by nuclear interactions of primary cosmic rays with nuclei in the atmosphere, almost atmospheric electrons are produced via atmospheric gamma rays from neutral pion decay. Komori *et al.* (2011) estimaed atmospheric electron spectra from the observed gamma-ray spectrum using a cascade shower theory [9].

We derived the cosmic-ray electron spectrum using the following formula:

$$J_{\rm e}(E) = \frac{N_{\rm e} - N_{\rm 2nd}}{S\Omega_e T \Delta E C_{\rm eff} C_{\rm enh}} ({\rm m}^{-2}{\rm s}^{-1}{\rm sr}^{-1}{\rm GeV}^{-1}). \quad (2)$$

Here, $N_{\rm e}$ is the number of the observed electron events, $N_{\rm 2nd}$ is the number of atmospheric electrons, $C_{\rm eff}$ is electron detection efficiency, and $C_{\rm enh}$ is enhancement factor due to the energy resolution. The electron detection efficiency $C_{\rm eff}$ is 1.00 for the emulsion chambers. The uncertainty of the energy determination has the effect of enhancing the absolute flux of electrons, in particular, for the steep power-law spectrum. The enhancement factor $C_{\rm enh}$ due to the energy resolution has values from 1.01 to 1.04, depending on electron energies.

4 Results and discussion

The total number of observed electrons is 166 events in the energy range from 30 GeV to 3 TeV. After the corrections described above, we derived the primary cosmic-ray electron energy spectrum. Figure 6 presents the observed electron spectrum, which is well represented by a power-law function of

$$J_{\rm e} = (1.39\pm0.23)\times10^{-4}(E/100{\rm GeV})^{-3.28\pm0.10}$$
$$({\rm m}^{-2}{\rm s}^{-1}{\rm sr}^{-1}{\rm GeV}^{-1}). \quad (3)$$

The cosmic-ray electrons observed with the balloon-borne emulsion chambers extend up to 3 TeV without cut off in the form of a power-law spectrum. The exponential cut-off energy is larger than 1.9 TeV (90 % C.L.) with a fixed power-law index of -3.28.

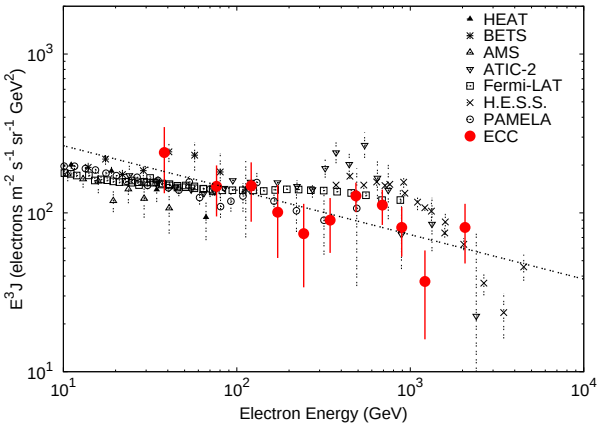

Figure 6: The primary cosmic-ray electron spectrum observed with ECC, compared to the previous experiments [6, 5, 10, and references therein]. The dotted line shows the best fitted power-law spectrum with an index of -3.28.

References

[1] T.Kobayaoshi, Y.Komori, K.Yoshida, and J.Nishimura, *Astrophys. J.*, 2004, **601**: 340-351
[2] H.C.Cheng, *et al.* , *Phys. Rev. Lett.*, 2002, **89**: 211301
[3] J.Chang, *et al.* , *Nature*, 2008, **456**: 362-365
[4] A.D.Panov, *et al.* , *Astrophys. Space Sci. Trans.*, 2011, **7**: 119-124
[5] M.Ackermann *et al.* (Fermi-LAT Collaboration), *Phys. ReV. D*, 2010, **82**:092004
[6] F.Aharonian *et al.* (H.E.S.S. Collaboration), *Astron. & Astrophys.*, 2009, **508**:561
[7] J.Nishimura *et al.* , 1980, *Astrophys. J.*, **238**:394-409
[8] K.Kasahara, *Epics Home Page*, 2010, http://cosmos.n.kanagawa-u.ac.jp/EPICSHome/
[9] Y.Komori *et al.* , 2011, *in preparation*
[10] O.Adriani *et al.* , *Phys. Rev. Lett.*, 2011, **106**:201101